ACS APPLIED MATERIALS & INTERFACES

Research Article

www.acsami.org

Conjugating *S*-Nitrosothiols with Glutathiose Stabilized Silver Sulfide Quantum Dots for Controlled Nitric Oxide Release and Near-Infrared Fluorescence Imaging

Lianjiang Tan,[†] Ajun Wan,*[,†] and Huili Li[‡]

[†]School of Chemistry and Chemical Engineering, Shanghai Jiao Tong University, Shanghai, 200240, China

[‡]School of Pharmacy, Shanghai Jiao Tong University, Shanghai, 200240, China

Supporting Information

ABSTRACT: Light-controllable nitric oxide (NO) delivery nanoparticles with the capability of near-infrared (NIR) fluorescence imaging were reported. Water-dispersible Ag_2S quantum dots (QDs) were synthesized via a one-pot procedure using reduced glutathiose (GSH) as both sulfur source and stabilizer. *S*-nitrosothiols (RSNOs) were conjugated with the GSH stabilized Ag_2S QDs at the amino groups of the GSH, leading to Ag_2S-GSH-SNO nanoparticles with dimension of ~5.5 nm. The biocompatible Ag_2S-GSH-SNO nanoparticles could release NO under UV or visible irradiation and emit NIR fluorescence under NIR excitation for bioimaging at physiological pH and temperature, yet could hardly release NO when NIR irradiation was applied. In vitro cell imaging and mice imaging experiments demonstrated that the Ag_2S-GSH-SNO nanoparticles could emit readily observable NIR fluorescence and release NO in living cells and small animals. The NIR fluorescence imaging of the Ag_2S-GSH-SNO nanoparticles would not interfere with the light-triggered NO release from them, as the excitation lights needed for these two functions were in different wavelength regions. This work provides new perspectives for the application of multifunctional nanostructured materials in diagnostics and imaging.

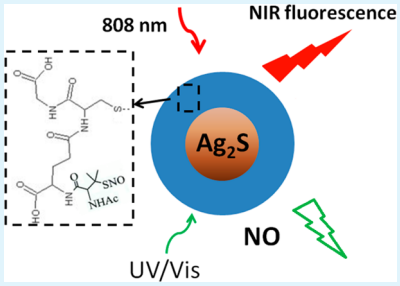

KEYWORDS: *S-nitrosothiols, silver sulfide quantum dots, nitric oxide, near-infrared imaging*

1. INTRODUCTION

As a new class of fluorescent probes, quantum dots (QDs), are currently under intensive studies in bioimaging and biosensing.[1−4] For in vivo fluorescence imaging, near-infrared (NIR) fluorescent quantum dots possess superior properties over those emitting in visible region due to reduced albedo and autofluorescence in this wavelength region, as well as great penetration depth for deep tissue imaging with high feature fidelity.[5,6] A variety of NIR fluorescent QDs have been successfully designed, such as PbS, PbSe, and certain heterostructured QDs.[7−10] These Cd-, Pb-, or Hg-containing QDs, however, are intrinsically toxic, which limits their use for in vivo applications. Nanoscaled silver chalcogenides, which have low toxicity and narrow band gaps are promising candidates for NIR QDs in recent years.[11−14] In some studies, NIR fluorescent silver sulfide (Ag_2S) QDs synthesized in organic phase exhibited tunable optical properties and good biocompatibility.[15,16] Ag_2S has an ultralow solubility product constant (K_{sp} = 6.3 × 10^{-50}), which ensures the minimum amount of Ag ion leaked into the biological surroundings.[17] More recently, functionalized Ag_2S QDs used for targeted small animal imaging have been reported.[18−20] The water-dispersible Ag_2S QDs synthesized with facile methods served as excellent NIR imaging agents, which provides new perspectives for nanodiagnostics and imaging in vivo.

Nitric oxide (NO), a free radical molecule possessing very important functions in biological systems, is generated in various tissues from the amino acid L-arginine by different forms of nitric oxide synthase.[21] To develop its applications in regulation of blood pressure, immune response, and neural communication, various exogenous NO donors have been designed and synthesized. We have developed chitosan-based NO donors that can spontaneously release NO molecules in physiological environment and simultaneously detect the NO release in situ with the aid of conjugated fluorescent agents.[22,23] It is imperative, however, for a therapeutic NO delivery system to be capable of controlled NO release.[24] In addition, incorporation of fluorophores that are highly effective for in vivo fluorescence imaging is urgent need for therapeutic applications of NO donors.

Currently, controlled delivery of NO from fluorescent complexes with low cytotoxicity and ability of efficient cell uptake is still challenging. There have been very few reports concerning controllable NO release from biocompatible NIR fluorescent vehicles. Herein we report a light-responsive NO releasing nanosystem capable of NIR fluorescence imaging for therapeutic applications. As depicted in Figure 1, reduced glutathiose (GSH) stabilized Ag_2S QDs were first synthesized in hot water via a simple one-pot route, with the GSH serving as both sulfur source and stabilizer. The reaction time affected

Received: August 15, 2013
Accepted: October 11, 2013
Published: October 11, 2013

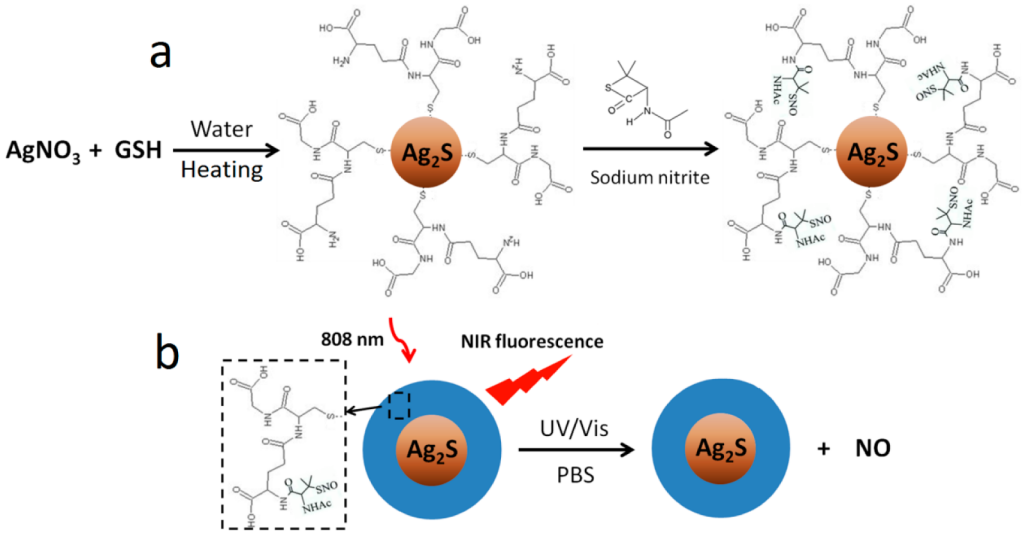

Figure 1. (a) Synthetic strategy of Ag_2S-GSH-SNO nanoparticles. (b) Schematic presentation of light-triggered NO release and NIR fluorescence imaging of Ag_2S-GSH-SNO nanoparticles.

the fluorescence properties of synthesized Ag_2S QDs (Supporting Information (SI) Figure 1s). *S*-Nitrosothiols (RSNOs), which are generally viewed as the reservoir for NO,[25,26] were then conjugated to the GSH-stabilized Ag_2S QDs at the primary amino site. The resultant Ag_2S-GSH-SNO nanoparticles possessed the functions of UV or visible light controlled NO release and NIR fluorescence imaging. The characteristics of controllable NO delivery, highly effective fluorescence imaging and small size, make the nanovehicles advantageous over those reported in our previous work.[22,23]

2. EXPERIMENTAL SECTION

Materials. Silver nitrate ($AgNO_3$), sodium nitrite, hydrochloric acid (1 M), methylene chloride, and acetic anhydride were all provided by Sinopharm Chemical Reagent Co., Ltd., China. *N*-acetyl-D,L-penicillamine, glutathiose (GSH), pyridine, indocyanine green (ICG), and RPMI 1640 cell culture medium were all purchased from Sigma Aldrich. Fetal bovine serum (FBS) was purchased from Institute of Biochemistry and Cell Biology, CAS. PBS (phosphate buffered saline) buffers (0.01 and 0.2 M, pH = 7.4) were prepared in our own lab. All chemicals were analytical grade unless otherwise stated.

One-Pot Synthesis of GSH Stabilized Ag_2S Quantum Dots. In a typical synthetic procedure, 50 μmol of $AgNO_3$ and 50 μmol of GSH (molar ratio = 1:1, with 2:1 and 1:2 for comparison) were dissolved in 10 mL of deionized water in a three-neck flask at 80 °C under argon flow, stirred at this temperature for 10 min to form a white cloudy mixture. The mixture was then heated to 95 °C and held under vigorous stirring for 2 h (with 1 and 3 h for comparison), changing from white cloudy to yellow clear and finally to dark yellow. Once the reaction was finished, the mixture was cooled to room temperature and was dialyzed against deionized water for 24 h to remove unreacted molecules and ions. The resultant colloidal solution was aqueous solution of Ag_2S QDs stabilized by GSH.

Preparation of Ag_2S-GSH-SNO Nanoparticles. The amino groups of GSH were the reactive sites for the formation of *S*-nitrosothiols. A 1.22 g portion of *N*-acetyl-D,L-penicillamine was dissolved in 2.5 mL of pyridine at 0 °C under stirring, followed by the addition of 2.5 mL of acetic anhydride for reaction at 25 °C for 24 h. The product was heated to 60 °C under the condition of reduced pressure to remove the pyridine and then washed and dried to produce thiolactone. A 46 mg portion of thiolactone was added to 15 mL of methylene chloride, followed by adding 69 mg of GSH-Ag_2S QDs. The mixture was stirred at 25 °C for 5 h under the protection of nitrogen. The resultant products were centrifuged, washed by methylene chloride, and vacuum-dried at 25 °C to form Ag_2S-GSH-SH nanoparticles. A 50 mg portion of Ag_2S-GSH-SH was added to 2 mL of methanol at 0 °C under stirring. Then 1 mL of hydrochloric acid (1 M) was added under stirring, followed by dropwise addition of 1 mL of sodium nitrite aqueous solution (0.5 M) at 0 °C. The mixture was allowed to react for 30 min. The resultant Ag_2S-GSH-SNO nanoparticles were centrifuged for 10 min, washed by methanol, and vacuum-dried at 25 °C for 3 h.

Characterization. Fourier transform infrared spectroscopy (FTIR) tests were conducted on a Spectrum 100 FTIR spectrometer (PerkinElmer, US). Samples were dried, powdered, and made into films by mixing them with KBr. The formation of *S*-nitrosothiols was identified on an AVANCE III NMR spectrometer (Bruker, Switzerland) at 400 MHz. Chemical shifts are given in parts per million relative to neat nitromethane (δ = 0) as the external standard. Transmission electron micrographs (TEM) were recorded on a JEM-2100 transmission electron microscope (JEOL, Japan) at 200 kV. Samples were suspended in ethanol, fully dispersed by ultrasonic wave, and deposited on an amorphous carbon coated copper grid prior to observation. The JEM-2100 transmission electron microscope equipped with EDX spectrometry was also used for the energy-dispersive X-ray (EDX) analysis. Surface analysis was conducted on an ESCALAB 250 X-ray photoelectron spectrometer (XPS, Thermo Scientific, US) with nonmonochromatic Al Kα X-ray (1486.6 eV). The analyzer was operated at 20 eV pass energy with an energy step size of 1 eV (full spectra) and 0.1 eV (high resolution spectra). Binding energy calibration was based on C 1s at 284.6 eV. Powder X-ray diffraction (XRD) patterns were collected using a D/max-2200/PC X-ray diffractometer (Rigaku, Japan) fitted with nickel-filtered Cu Kα radiation. The data were collected at 0.02° intervals with counting for 0.2 s at each step. The size distribution of the Ag_2S-GSH-SNO nanoparticles were determined by a Nano ZS90 particle size and zeta potential analyzer (Malvern, UK) based on dynamic light scattering (DLS) at a scattering angle of 90°. UV−vis-NIR absorption spectra were recorded by a Lambda 750S UV−vis-NIR spectrophotometer (PerkinElmer, US), background corrected for any water contribution. NIR fluorescence spectra were collected on a Fluorolog-3 fluorescence spectrophotometer (Horiba Jovin Yvon, France) equipped with a liquid nitrogen cooled InGaAs detector (800−1600 nm), applying the excitation laser of 808 nm. NIR images of the Ag_2S-GSH-SNO nanoparticles in PBS buffer and mouse whole blood were acquired under 808 nm using a liquid nitrogen cooled two-dimensional InGaAs camera (Princeton Instruments, US) with a sensitivity ranging from 800 to 1700 nm. The images were analyzed with the image processing software *Image J* (National Institutes of Health, US). The concentration of Ag_2S-GSH-SNO nanoparticles was determined on

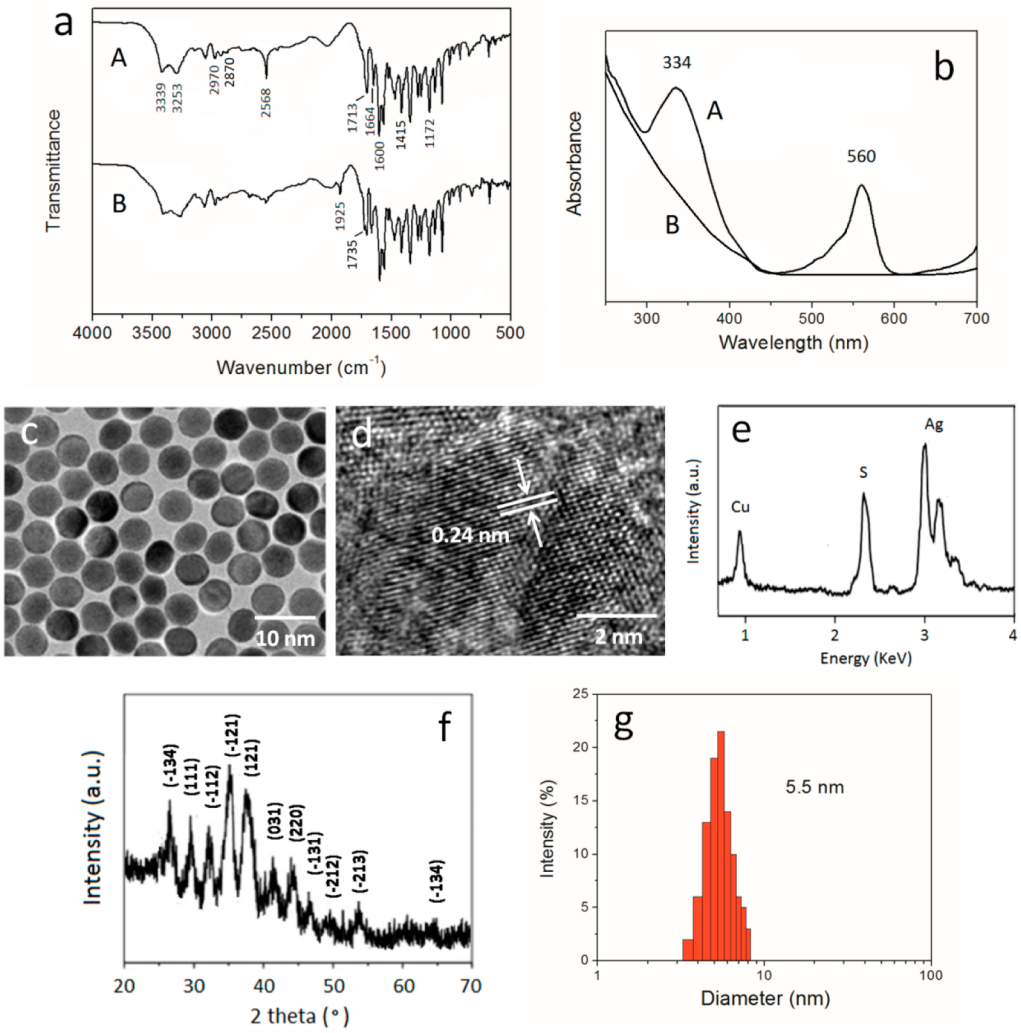

Figure 2. (a) FTIR spectra of **A** GSH and **B** Ag_2S-GSH-SNO nanoparticles. (b) UV–vis spectra of **A** Ag_2S-GSH-SNO nanoparticles and **B** Ag_2S-GSH nanoparticles in water. (c) TEM micrograph, (d) high-resolution TEM micrograph, and (e) EDX spectrum of as-prepared Ag_2S-GSH-SNO nanoparticles. (f) XRD pattern and (g) size distribution of as-prepared Ag_2S-GSH-SNO nanoparticles.

an X series inductively coupled plasma mass spectrometer (ICP-MS) (Thermo Elemental, UK).

Determination of the Quantum Yield of Ag_2S-GSH-SNO Nanoparticles. The quantum yield of the as-prepared Ag_2S-GSH-SNO nanoparticles was measured using indocyanine green (ICG) as a reference (QY = 13% in DMSO). The absorption spectra of Ag_2S-GSH-SNO nanoparticles and ICG solutions at different concentrations were recorded. Then, the fluorescence spectra of these samples were recorded under the same conditions. The fluorescence quantum yield was calculated according to the following equation:

$$\phi_{NS} = \phi_{ICG}\left(\frac{F_{NS}}{F_{ICG}}\right)\left(\frac{A_{ICG}}{A_{NS}}\right)\left(\frac{n_{NS}}{n_{ICG}}\right)^2 \quad (1)$$

Where ϕ_{NS}, F_{NS}, A_{NS}, and n_{NS} are the quantum yield, integrated fluorescence intensity, integrated absorption, and refractive index of the solvent for the Ag_2S-GSH-SNO nanoparticles. The parameters with a subscript of ICG are corresponding quantities of the solvent for ICG.

Measurement of NO Release. Quantitative detection of the NO molecules released from the Ag_2S-GSH-SNO nanoparticles was carried out by a TBR 4100/1025 free radical analyzer equipped with an ISO-NOP sensor (WPI Ltd., US). The sensor was calibrated by the addition of 50 μM KNO_2 in a mixture of 0.33 g KI and 20 mL of 0.1 M H_2SO_4. The NO release was measured at 37 °C, where the detection sensitivity was determined to be 2.55 pA/nM. The details are as follows: 0.1 mg of nanoparticles was dispersed in 1 mL of a 0.2 M PBS buffer (pH = 7.4), forming a stable suspension. Then, the suspension was rapidly injected into 19 mL of the PBS buffer when the ISO-NOP sensor had reached a low, stable current level. The NO probe was immersed about 2 cm into the suspension under magnetic stirring.

Cell Assay. L929 cells (mouse fibroblast cells) purchased from Institute of Biochemistry and Cell Biology, CAS, were cultured in RPMI 1640 medium supplemented with 10 wt % FBS, 100 IU/mL penicillin, and 100 μg/mL streptomycin in a humidified incubator with 5 vol% carbon dioxide at 37 °C. The medium was refreshed every 2 or 3 days according to cell density.

Cytotoxicity of the Ag_2S-GSH-SNO nanoparticles was evaluated by 3-(4,5-dimethylthiazole-2-yl)-2,5-diphenyltetrazolium chloride (MTT) viability assay. The L929 cells were seeded in 96-well culture plates at a density of 4200 cells per well and incubated at 37 °C for 24 h for cell attachment. The culture medium in each well was then replaced by a fresh medium containing the Ag_2S-GSH-SNO nanoparticles at different concentrations (0.01–1 mg/mL). One row of the 96-well plates was used as control. After further incubation for 24 or 48 h, the culture plates were rinsed with a 0.01 M PBS buffer (pH = 7.4) to remove unattached cells and the remaining cells were treated with 5 mg mL^{-1} MTT stock solution in PBS for 4 h. The medium containing unreacted MTT was then carefully removed. The obtained formazan was dissolved in DMSO, and the absorbance of individual wells was recorded at 570 nm using a Multiskan MK3 Enzyme-labeled

dx.doi.org/10.1021/am4034153 | ACS Appl. Mater. Interfaces 2013, 5, 11163–11171

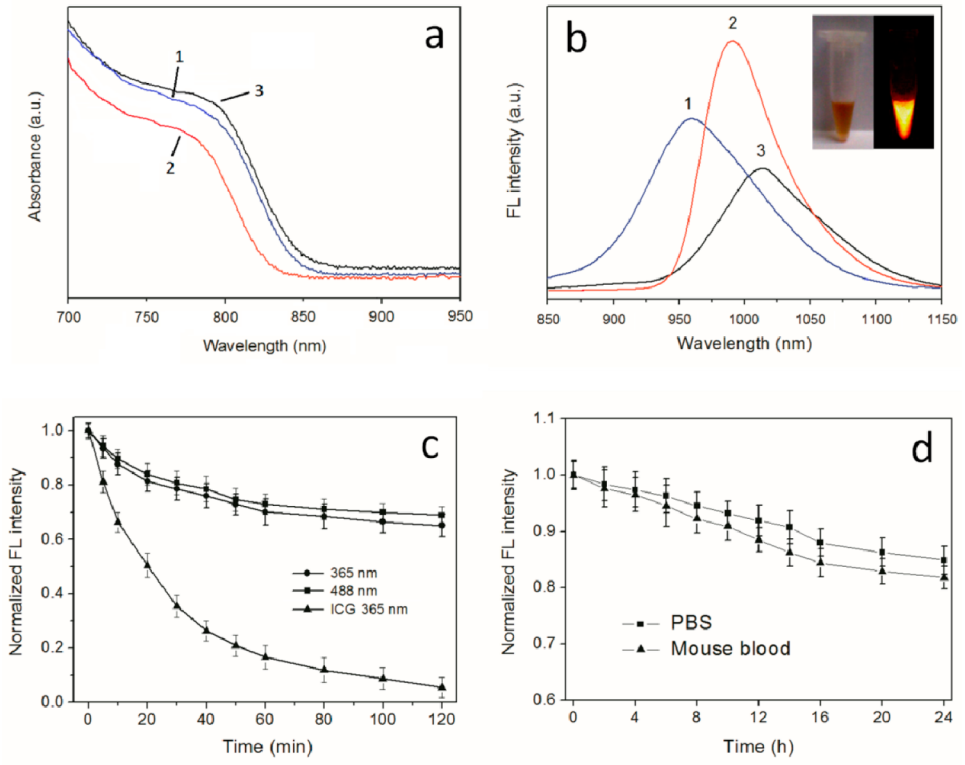

Figure 3. (a) Vis-NIR absorption spectra and (b) fluorescence spectra of Ag_2S-GSH-SNO nanoparticles fabricated at the molar ratio of $AgNO_3$ to GSH equal to **1** 2:1; **2** 1:1; **3** 1:2. (inset) Bright-field (left) and NIR fluorescence (right) images of Ag_2S-GSH-SNO nanoparticles under 808 nm excitation. (c) Photostability of the GSH stabilized Ag_2S QDs (under irradiation of 365 and 488 nm laser) in comparison to ICG (under irradiation of 365 nm laser). The irradiation power was 100 W. (d) Photostability of Ag_2S-GSH-SNO nanoparticles in PBS buffer (pH = 7.4) and mouse whole blood at 37 °C.

Instrument (Thermo Scientific, US). The cell survival rate was determined by the following equation:

$$\text{cell survival rate } \% = \text{absorbance of test cells} / \text{absorbance of control cells} \times 100\% \quad (1)$$

In vitro Cell Imaging. A suspension of L929 cells incubated with 0.1 mg/mL Ag_2S-GSH-SNO nanoparticles for 3 h was transferred to an eight-well Lab-Tek II chamber slide (Nalge Nunc, Napevillem, IL). The medium was then aspirated from the wells, and the cells were rinsed with fresh medium three times before observation. NIR cell imaging was performed using the liquid nitrogen cooled InGaAs camera. The excitation light was provided by an 808 nm laser diode and the emitted photons were collected in the 900−1700 nm NIR range using a 900 nm long-pass filter.

Imaging of Intracellular NO Release. L929 cells were incubated with Ag_2S-CS-SNO nanospheres (0.1 mg/mL) for 5 h. After thorough washing with fresh culture medium, 10 μg of Cu-2-{2-chloro-6-hydroxy-5-[(2-methyl-quinolin-8-ylamino)-methyl]-3-oxo-3*H*-xanthen-9-yl}-benzoic acid (CuFL) was added and incubated for 2 h at 37 °C. Then the cells were rinsed three times with fresh culture medium. The cell fluorescence was observed by a confocal laser scanning microscope (Zeiss LSM 710, Germany) equipped with a 488 nm excitation source by the green channels. The 488 nm laser served as both NO triggering and exciting source.

In vivo and ex vivo Imaging. Animal procedures were carried out according to protocols approved by the Animal Ethics Committee of the Institute of Hematology and Hospital of Blood Diseases, Chinese Academy of Medical Sciences and Peking Union Medical College. Nude mice (~20 g) purchased from Laboratory Animal Center of Nanjing Medical University were anesthetized with 10% chloral hydrate via intraperitoneal injection. Then 5 μg of Ag_2S-GSH-SNO nanoparticles (0.1 mg/mL in PBS) were injected into tail vein or subcutaneous tissue of the nude mice. After certain periods of time, the mice were positioned on an imaging platform, and NIR fluorescence images were collected using the liquid-nitrogen-cooled InGaAs camera. The major organs were removed from the mouse following tail vein injection for ex vivo imaging. The excitation light was provided by an 808 nm laser diode coupled to a 4.5 mm focal length collimator. The emitted light from the animal was filtered through a 900 nm long-pass filter coupled with the InGaAs camera for NIR imaging. The excitation power density at the imaging plane was 140 mW/cm^2. In another imaging experiment, 0.5 μg of CuFL and 3 μg of Ag_2S-GSH-SNO nanoparticles were injected subcutaneously to anesthetized mice. The mice were imaged using a Maestro in vivo optical imaging system (CRI Inc., US) at 5 min postinjection. The excitation wavelength was set at 488 nm. The emission was filtered by a 500−600 nm band-pass filter.

3. RESULTS AND DISCUSSION

Structure and Morphology. Fourier transform infrared (FTIR) spectroscopy was used to identify the chemical structure of our synthetic product. In Figure 2a, the FTIR spectrum of GSH (A) shows an absorption peak at 2568 cm^{-1}, characteristic of free thiol group. The peak at 1713 cm^{-1} is ascribed to the C═O stretch vibration of carboxyl group, while the one at 1664 cm^{-1} corresponds to the C═O stretching of amide (amide I). The peaks at 1415 and 1303 cm^{-1} are assigned to the amide II and amide III bands. For the Ag_2S-GSH-SNO nanoparticles, the absorption appearing at 1925 cm^{-1} indicated the formation of —SNO groups[27] in the nanoparticles. A new peak at 1735 cm^{-1} is attributable to the C═O stretching of the ester groups in RSNOs. The peak at 2548 cm^{-1} greatly diminished compared with GSH, since the thiols were consumed and the GSH was bound to the surface of

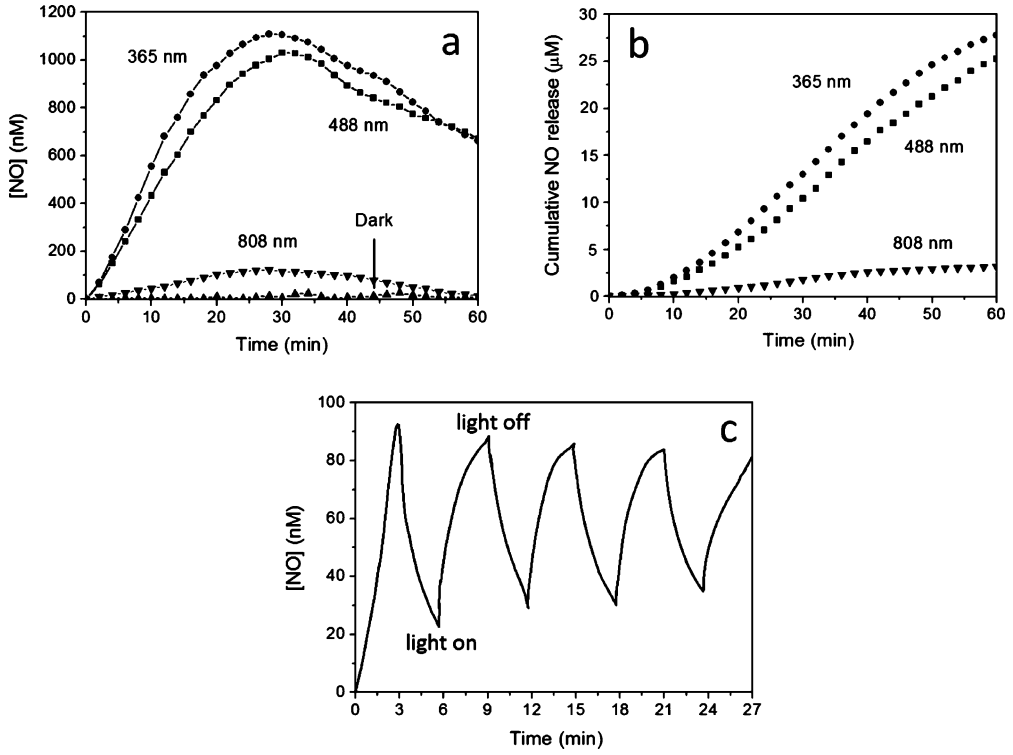

Figure 4. (a) Real-time NO generation from Ag_2S-GSH-SNO nanoparticles in a PBS buffer (pH = 7.4, 37 °C) triggered by light of different wavelengths. (b) Cumulative NO release profiles of Ag_2S-GSH-SNO nanoparticles in the PBS buffer obtained based on the data in part a. (c) Controlled on-and-off NO release behavior of Ag_2S-GSH-SNO nanoparticles by 488 nm light in the PBS buffer. The on−off−on cycle was set at 6 min. The laser power applied was 30 W.

Ag_2S QDs via the Ag-thiol bond. The UV−vis absorption spectra of Ag_2S-GSH-SNO and Ag_2S-GSH nanoparticles are shown in Figure 2b. For the Ag_2S-GSH-SNO nanoparticles, a strong absorption at 334 nm is attributed to the $n_0 \rightarrow \pi^*$ electronic transition, which is common to RSNOs.[28] Another absorption peak situated at 560 nm is ascribed to the $n_N \rightarrow \pi^*$ electronic transition of RSNOs. In comparison, the Ag_2S-GSH nanoparticles showed only a relatively weak absorption at ∼425 nm. These results confirm the formation of RSNOs in Ag_2S-GSH-SNO nanoparticles. Nitrogen NMR technique is an effective tool in both organic chemistry and biochemistry. The ^{15}N NMR spectrum of the Ag_2S-GSH-SNO nanoparticles shows a sharp peak at 791.8 ppm (Figure 2s, SI), further confirming the existence of RSNOs.[29]

The morphology of as-prepared Ag_2S-GSH-SNO nanoparticles was observed by TEM. Figure 2c presents the monodisperse nanoparticles. The high-resolution TEM micrograph in Figure 2d shows lattice fringes of the nanocrystals with an interplanar spacing of ∼0.24 nm, which could be assigned to the (−1, 1, 2) facets of monoclinic α-Ag_2S crystal. Energy dispersive X-ray (EDX) analysis in Figure 2e indicates the presence of elements Ag and S in the nanoparticles with atomic ratio a little smaller than the stoichiometry of bulk Ag_2S. The X-ray photoelectron spectroscopy (XPS) results (Figure 3s, SI) indicate that the oxidation state of Ag ion was univalent in the Ag_2S QDs. In the X-ray diffraction (XRD) pattern of the nanoparticles (Figure 2f), the positions and relative intensities of the diffraction peaks matched monoclinic Ag_2S. The broadening of the peaks compared with the pattern of bulk Ag_2S (Figure 4s, SI) may suggest the nanocrystalline nature of the sample. The size distribution histogram for the nanoparticles in Figure 2g reflects the average diameter of 5.5 nm. By tuning the precursor molar ratio of $AgNO_3$ to GSH (2:1 and 1:2), uniform Ag_2S-GSH-SNO nanoparticles were obtained with varied average diameters (Figure 5s SI).

Optical Properties. The optical properties of the Ag_2S-GSH-SNO nanoparticles were investigated. The vis-NIR absorption spectra in Figure 3a show a characteristic absorption at 780−800 nm. The molar ratio of $AgNO_3$ to GSH seemed not to exert significant influence on the optical absorption of the nanoparticles. In Figure 3b, the fluorescence emission peak of the nanoparticles shifted from 960 to 990 nm and to 1015 nm in the NIR region as the $AgNO_3$ to GSH molar ratio decreased from 2:1 to 1:1 and to 1:2, giving the fluorescence quantum yield values (QY, determined against indocyanine green) of 1.35%, 1.97%, and 0.96%, respectively. The nanoparticles with the QY = 1.97% were suitable for NIR imaging in vivo. The emission peak at 990 nm had a full width at half-maximum of 68 nm, signifying a narrow size distribution of the nanoparticles. A large Stokes shift (∼200 nm) helps to enhance the fluorescence imaging quality of the nanoparticles. The observed emission from the nanoparticles was in the near-infrared region (Figure 3b, inset). Subject to visible light irradiation, the nanoparticles would release NO and meanwhile emit NIR fluorescence. The generated NO molecules may change the surface states of the nanocrystals. We compared the fluorescence emissions of the Ag_2S-GSH-SNO nanoparticles with the Ag_2S-GSH nanoparticles after 488 nm irradiation for 20 min and found that the difference in the emission intensity between them was 6% (Figure 6s, SI). Therefore, the influences of released NO on the NIR fluorescence of the Ag_2S-GSH-SNO nanoparticles were tiny. The photostability of GSH stabilized Ag_2S QDs was examined (Figure 3c). The QDs retained 65% and 69% of the original fluorescence after 120

min of 365 and 488 nm irradiation, respectively, whereas the organic NIR fluorescent ICG was almost photobleached within the same period. In PBS or mouse whole blood, the nanoparticles exhibited no obvious decrease in fluorescence and maintained over 80% of the original intensity after 24 h (Figure 3d). These results indicate good chemical stability and photostability of the nanoparticles.

Light-Controlled NO Release. To investigate the NO release from the Ag_2S-GSH-SNO nanoparticles induced by light, quantitative detection of released NO was conducted. Figure 4a shows the instant NO generation versus time curves for the Ag_2S-GSH-SNO nanoparticles in PBS buffer under varied conditions. The nanoparticle samples excited by 365 nm UV light and 488 nm visible light exhibited release of NO at an increasing rate during the initial 30 min, after which a gradual decrease in the instant NO release was observed for both the two samples. The sample excited by 808 nm NIR laser also showed NO release, yet at a much lower level. Another sample hardly released detectable NO in the absence of irradiation. We could then exclude uncontrolled NO release caused by Ag or ambient ions and ensure the dose of NO delivered to target cells or tissues by the nanoparticles. The cumulative NO release profiles under irradiation of different wavelengths determined by the instant NO generation at each time point are depicted in Figure 4b. Irradiated by 365 or 488 nm light, NO was released steadily from the nanoparticles in the data range, reaching a dose of over 25 μM at 60 min. When 808 nm NIR light was applied, only a fairly small amount of NO was generated (about 3 μM at 60 min). It is evident that the NO release from the Ag_2S-CS-SNO nanospheres needed light triggering in UV or visible region, and the NIR light could not induce substantial NO release. Although more NO was released under 365 nm irradiation, the 488 nm light was preferred in therapy since it causes less injury to tissues. The off-and-on behavior of NO release controlled by 488 nm light was illustrated in Figure 4c. The "zig-zag" release profile indicates fast response of the nanoparticles to the triggering light. In addition, the NO release showed little fatigue effect under the repeated off-and-on control.

Intracellular NO Release and Cell Imaging. We performed cell imaging and small animal imaging to demonstrate the fluorescence imaging ability of the Ag_2S-GSH-SNO nanoparticles. Also, intracellular NO release of the Ag_2S-GSH-SNO nanoparticles under 488 nm irradiation was measured. First the MTT assay was used to examine the accurate cytotoxicity of the Ag_2S-GSH-SNO nanoparticles (Figure 5). At a high concentration of 1.0 mg/mL, 86% and 82% of the cells survived relative to the control group after incubation for 24 and 48 h, respectively, suggesting the low cytotoxicity of the Ag_2S-GSH-SNO nanoparticles. In vitro cell imaging for the Ag_2S-GSH-SNO nanoparticles was illustrated in Figure 6a–c. The L929 cells were incubated with the Ag_2S-GSH-SNO nanoparticles for 3 h to allow internalization of the nanoparticles in the cells. The small size of the nanoparticles favored quick cell uptake. NIR fluorescence was emitted from the cells immediately upon irradiation of 808 nm laser. The nanoparticles displayed a punctuated cytoplasmic distribution, indicative of confinement in endosomes and lysosomes as common for QDs. After continuous irradiation for 2 h, the fluorescence of the cells did not show appreciable decrease. Furthermore we introduced a synthesized fluorescence agent, NO-sensitive CuFL,[23] into the nanoparticle-containing cells for confocal imaging of NO. The 488 nm light was used as both

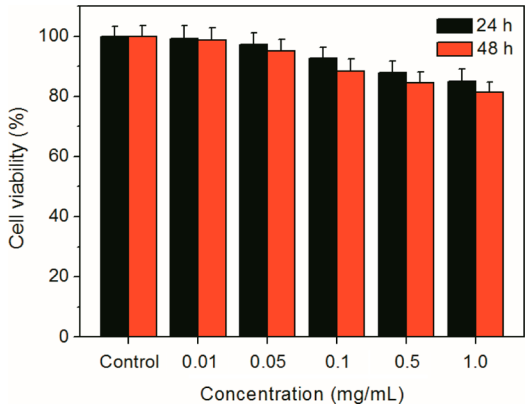

Figure 5. Viability of L929 cells incubated with different concentrations of Ag_2S-GSH-SNO nanoparticles. The cells without treatment of Ag_2S-GSH-SNO nanoparticles were used as controls.

triggering source for NO release and excitation source for the CuFL. As shown in Figure 6d, green fluorescence characteristic of the CuFL encountering NO appeared upon irradiation, indicating quick NO release from the nanoparticles in the cells. In comparison, the cells without nanoparticles and containing Ag_2S-GSH nanoparticles (no release of NO) showed no visible fluorescence signal (Figure 6e and f). It can be concluded that the nanoparticles are capable of releaseing NO in living cells. The NIR image of the cells in Figure 6d (Figure 6g) and the corresponding overlay image (Figure 6h) further confirmed the release of NO from the nanoparticles.

Small Animal Imaging Studies. In vivo imaging of nude mice was performed to demonstrate potential therapical applications of the Ag_2S-GSH-SNO nanoparticles. A 5 μg dose of the nanoparticles (0.1 mg/mL in PBS) was administered into anesthetized nude mice by tail vein injection. At different time points postinjection, the mice were imaged under 808 nm excitation. As shown in Figure 7a, the NIR fluorescence signals derived from the nanoparticles in the mice body were visualized at 1 h postinjection. At longer time postinjection, the nanoparticles were distributed in several regions of the mice body via blood circulation (Figure 7b and c). The NIR signals were still detectable after up to 24 h (Figure 7d), indicating slow clearance of the nanoparticles in the mice. Especially at the liver site, the fluorescence maintained at a high level at 24 h postinjection. The good contrast of the images due to deep tissue penetration of the NIR fluorescence facilitates diagnosis and treatment monitoring. The readily detectable signals further indicated the strong tissue penetrability of the NIR fluorescence emitted by the nanoparticles. Furthermore, ex vivo NIR imaging was conducted for a nude mouse following the in vivo NIR imaging. Figure 7e shows an ex vivo NIR image of the viscera harvested from a sacrificed mouse at 12 h after administration of the Ag_2S-GSH-SNO nanoparticles. The NIR signals were clearly detected in the liver, stomach, and spleen, and the fluorescence intensities of the lung and kidney were poor. We can thus deduce that the Ag_2S-GSH-SNO nanoparticles tend to be enriched in the liver, stomach, and spleen. NO release from the nanoparticles in nude mice was evidenced. Both CuFL and the nanoparticles were administered to the mice via subcutaneous injection to facilitate observation. As displayed in Figure 7f and g, the injection region of a mouse emitted fluorescence under 488 nm irradiation at 5 min postinjection, which indicated the in vivo NO release from the nanoparticles.

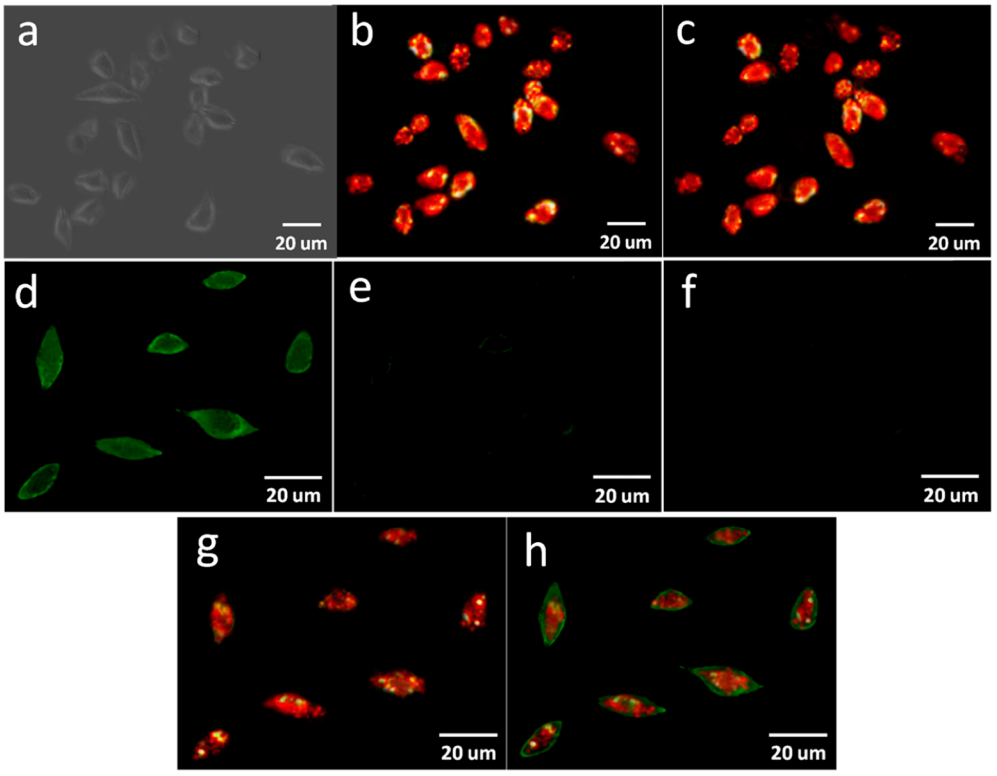

Figure 6. (a) Bright-field image, (b) NIR image acquired immediately upon 808 nm irradiation, and (c) NIR image acquired after 808 nm irradiation for 2 h of L929 cells incubated with 0.1 mg/mL Ag_2S-GSH-SNO nanoparticles for 3 h. CLSM images (488 nm excitation) of the NO detection of CuFL stained cells after incubation with the Ag_2S-GSH-SNO nanoparticles for 3 h (d), after incubation with the Ag_2S-GSH nanoparticles for 3 h (e), and without containing any nanoparticles (f). (g) NIR image and (h) overlay image (CLSM and NIR) of the CuFL stained cells after incubation with the Ag_2S-GSH-SNO nanoparticles for 3 h.

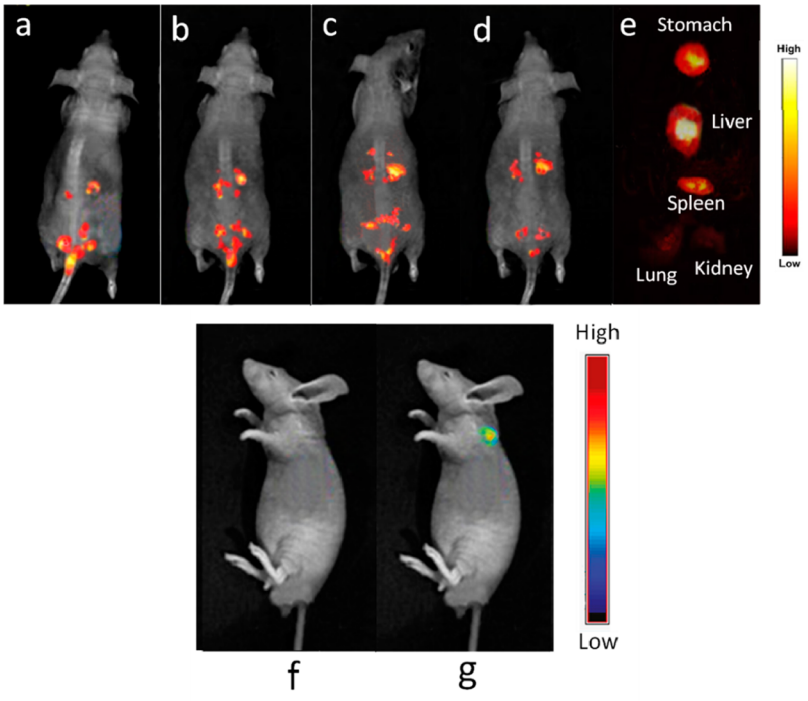

Figure 7. In vivo NIR images of nude mice at 1 (a), 6 (b), 12 (c) and 24 h (d) after tail intravenous injection of Ag_2S-GSH-SNO nanoparticles. (e) Ex vivo NIR images of viscera from a sacrificed nude mouse at 12 h postinjection. (f) Bright-field image and (g) fluorescence image of a nude mouse at 5 min after subcutaneous injection of CuFL and Ag_2S-GSH-SNO nanoparticles under irradiation of 488 nm laser.

The distribution of the nanoparticles in viscera was evaluated using inductively coupled plasma-mass spectroscopy (ICP-MS) (Figure 8a). Most of the nanoparticles were accumulated in the liver, stomach, spleen, and blood 12 h postadministration. The

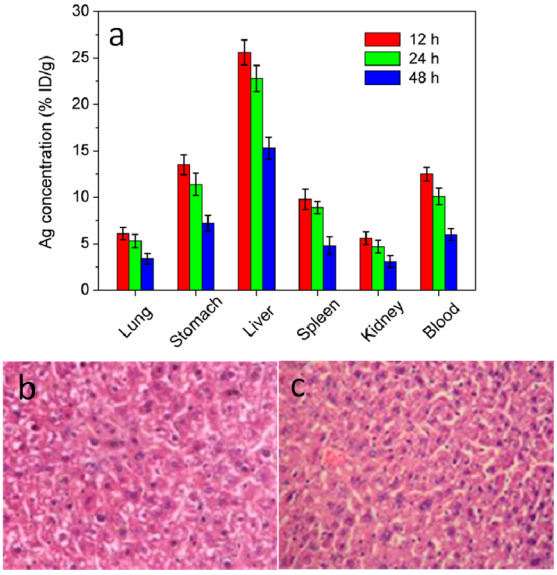

Figure 8. (a) In vivo biodistribution and toxicity analysis of Ag_2S-GSH-SNO nanoparticles over a period of 48 h in a nude mouse. The Ag concentration in the organs was determined at different time points after tail intravenous injection of the Ag_2S-GSH-SNO nanoparticles (5 μg) using ICP-MS. Here % ID/g indicates the Ag element concentration in terms of the percentage of the injected dose (ID) per gram of tissue. Stained liver tissue sections from the nude mouse (b) without injection and (c) 12 h postinjection of Ag_2S-GSH-SNO nanoparticles. The tissue images are acquired at the magnification of 400.

nanoparticle content in the liver showed the highest level, indicating relatively high affinity of the nanoparticles for liver. With prolonged time, the nanoparticles were metabolized and their content in the mouse body decreased. Histological analysis of the liver was also carried out to evaluate the acute toxicity of the nanoparticles. Digital microscopy images show the pathological sections for a treated mouse and a control mouse (Figure 8b and c). Compared with the pathological section of the control mouse, no significant inflammatory morphology or density changes of the liver tissue was observed for the mouse subject to the injection of the nanoparticles at a dose level of 0.25 mg/kg. The results further suggest that the Ag_2S-GSH-SNO nanoparticles could be safely employed as a bioimaging and NO delivery agent.

4. CONCLUSIONS

To sum up, GSH stabilized Ag_2S QDs with RSNOs conjugated have been fabricated via a facile technique. Water-dispersible Ag_2S QDs were one-pot synthesized using GSH as both sulfur source and stabilizer. RSNOs were conjugated with the GSH stabilized Ag_2S QDs at the amino site to fabricate Ag_2S-GSH-SNO nanoparticles. The biocompatible Ag_2S-GSH-SNO nanoparticles are capable of releasing NO irradiated by UV or visible light, and emitting NIR fluorescence under NIR excitation. These two functions can be performed without interference with each other, since the excitation lasers for the NO release and NIR imaging are in different wavelength regions. The unique feature endows the Ag_2S-GSH-SNO nanoparticles great potential as a NO delivery and fluorescence imaging platform for biomedical applications.

■ ASSOCIATED CONTENT

Supporting Information

Relevant experimental results and data not included in the manuscript. This material is available free of charge via the Internet at http://pubs.acs.org.

■ AUTHOR INFORMATION

Corresponding Author

*E-mail: wanajun@sjtu.edu.cn. Fax: 86-21-34201245. Tel.: 86-21-34201245.

Notes

The authors declare no competing financial interest.

■ ACKNOWLEDGMENTS

This work was financially supported by the Shanghai Postdoctoral Sustentation Fund (13R21413800 and 13R21413900), the China Postdoctoral Science Foundation (2013M531164), the National Natural Science Foundation (21076124 and 51173104), and the Nanometer Technology Program of Science and Technology Committee of Shanghai (11 nm0503500).

■ REFERENCES

(1) Giemans, B. N. G.; Adams, S. R.; Ellisman, M. H.; Tsien, R. Y. *Science* **2006**, *312*, 217−224.
(2) Clapp, A. R.; Medintz, I. L.; Uyeda, H. T. *J. Am. Chem. Soc.* **2005**, *127*, 18212−18221.
(3) Michalet, X.; Pinaud, F. F.; Bentolila, L. A.; Tsay, J. M.; Doose, S.; Li, J. J.; Sundaresan, G.; Wu, A. M.; Gambhir, S. S.; Weiss, S. *Science* **2005**, *307*, 538−544.
(4) Neuman, D.; Ostrowski, A. D.; Mikhailovsky, A. A.; Absalonson, R. O.; Strouse, G. F.; Ford, P. C. *J. Am. Chem. Soc.* **2008**, *130*, 168−175.
(5) Aswathy, R. G.; Yoshida, Y.; Maekawa, T.; Kumar, D. S. *Anal. Bioanal. Chem.* **2010**, *397*, 1417−1435.
(6) Welsher, K.; Liu, Z.; Sherlock, S. P.; Robinson, J. T.; Chen, Z.; Daranciang, D.; Dai, H. *Nat. Nanotechnol.* **2009**, *4*, 773−780.
(7) Bakueva, L.; Gorelikov, I.; Musikhin, S.; Zhao, X. S.; Sargent, E. H.; Kumacheva, E. *Adv. Mater.* **2004**, *16*, 926−929.
(8) Wehrenberg, B. L.; Wang, C.; Guyot-Sionnest, P. *J. Phys. Chem. B.* **2002**, *106*, 10634−10640.
(9) Blackman, B.; Battaglia, D. M.; Mishima, T. D.; Johnson, M. B.; Peng, X. *Chem. Mater.* **2007**, *19*, 3815−3821.
(10) Kim, J. S.; Cho, K. J.; Tran, T. H.; Nurunnabi, M.; Moon, T. H.; Hong, S. M.; Lee, Y. K. *J. Colloid Interface Sci.* **2011**, *35*, 3363−3371.
(11) de la Rica, R.; Velders, A. H. *J. Am. Chem. Soc.* **2011**, *133*, 2875−2877.
(12) Sahu, A.; Qi, L.; Kang, M. S.; Deng, D.; Norris, D. J. *J. Am. Chem. Soc.* **2011**, *133*, 6509−6512.
(13) Yarema, M.; Pichler, S.; Sytnyk, M.; Seyrkammer, R.; Lechner, R. T.; Fritz-Popovski, G.; Jarzab, D.; Szendrei, K.; Resel, R.; Korovyanko, O.; Loi, M. A.; Paris, O.; Hesser, G. *ACS Nano* **2011**, *5*, 3758−3765.
(14) Ma, X. H.; Zhao, Y. Y.; Jiang, X. Y.; Liu, W.; Liu, S. Q.; Tang, Z. Y. *Chem. Phys. Chem.* **2012**, *13*, 2531−2535.
(15) Du, Y.; Xu, B.; Fu, T.; Cai, M.; Li, F.; Zhang, Y.; Wang, Q. *J. Am. Chem. Soc.* **2010**, *132*, 1470−1471.
(16) Hong, G.; Robinson, J.; Zhang, Y.; Diao, S.; Antaris, A. L.; Wang, Q. *Angew. Chem., Int. Ed.* **2012**, *51*, 9818−9821.
(17) Zhang, Y.; Hong, G.; Zhang, Y.; Chen, G.; Li, F.; Dai, H.; Wang, Q. *ACS Nano* **2012**, *6*, 3695−3702.
(18) Wang, Y.; Yan, X. P. *Chem. Commun.* **2013**, *49*, 3324−3326.
(19) Jiang, P.; Zhu, C. N.; Zhang, Z. L.; Tian, Z. Q.; Pang, D. W. *Biomaterials* **2012**, *33*, 5130−5135.
(20) Yang, H. Y.; Zhao, Y. W.; Zhang, Z. Y.; Xiong, H. M.; Yu, S. N. *Nanotechnology* **2013**, *24*, 055706.

(21) Butler, A. R.; Williams, D. L. H. *Chem. Soc. Rev.* **1993**, *22*, 233−241.
(22) Tan, L.; Wan, A.; Li, H.; Lu, Q. *Acta. Biomater.* **2012**, *8*, 3744−3753.
(23) Tan, L.; Wan, A.; Li, H. *Analyst* **2013**, *138*, 879−886.
(24) Ostrowski, A. D.; Lin, B. F.; Tirrell, M. V.; Ford, P. C. *Mol. Pharmaceutics.* **2012**, *9*, 2950−2955.
(25) Hwang, S.; Meyerhoff, M. E. *J. Mater. Chem.* **2007**, *17*, 1462−1465.
(26) Peterson, L. A.; Wagener, T.; Sies, H.; Stahl, W. *Chem. Res. Toxicol.* **2007**, *20*, 721−723.
(27) Munro, A. P. *S-Nitrosothiols: novel decomposition pathways including reactions with sulfur and nitrogen nucleophiles*. Doctoral Thesis, Durham University: Durham, 1999.
(28) Williams, D. L. H. *Acc. Chem. Res.* **1999**, *32*, 869−876.
(29) Wang, K.; Hou, Y.; Zhang, W.; Ksebati, M.; Xian, M.; Cheng, J. P.; Wang, P. G. *Bioorg. Med. Chem. Lett.* **1999**, *9*, 2897−2902.